Role of β4* Nicotinic Acetylcholine Receptors in the Habenulo-Interpeduncular Pathway in Nicotine Reinforcement in Mice

Lauriane Harrington[2, 3], PhD, Xavier Viñals[1], PhD, Andrea Herrera-Solís[1], PhD, Africa Flores[1], M.Sci., Carole Morel[5], PhD, Stefania Tolu[5], PhD, Philippe Faure[5], PhD, Rafael Maldonado[1], PhD, Uwe Maskos[2, 3,*],DPhil, and Patricia Robledo[1, 4,*], PhD

[1]Laboratory of Neuropharmacology, Pompeu Fabra University (UPF), Barcelona, Spain

[2]Institut Pasteur, Unité Neurobiologie Intégrative des Systèmes Cholinergiques, Département de Neuroscience, F-75724 Paris cedex 15, France.

[3]CNRS, UMR 3571, F-75724 Paris cedex 15, France

[4]Integrative Pharmacology and Systems Neuroscience, IMIM-Hospital del Mar Medical Research Institute, Barcelona, Spain,

[5]Neurobiologie des Processus Adaptatifs, CNRS UMR 7102, Equipe Neurophysiologie et comportement (NPC), Université P. et M. Curie, Paris, France; 2CNR

*These authors equally supervised this work

Corresponding Author:

Patricia Robledo, PhD
Integrative Pharmacology and Systems Neuroscience
Neurosciences Research Programme, IMIM-Hospital del Mar Research Institute.
PRBB
Calle Dr. Aiguader 88
Barcelona 08003
SPAIN
probledo@imim.es
Tel: +34 93 316 0455
FAX: +34 93 316 0901

Running title: Interpeduncular β4-nicotinic receptors and nicotine reinforcement

ABSTRACT

Nicotine exerts its psychopharmacological effects by activating the nicotinic acetylcholine receptor (nAChR), composed of alpha and/or beta subunits, giving rise to a diverse population of receptors with a distinct pharmacology. β4-containing (β4*) nAChRs are located almost exclusively in the habenulo-interpeduncular pathway. We examined the role of β4* nAChRs in the medial habenula (MHb) and the interpeduncular nucleus (IPN) in nicotine reinforcement using behavioral, electrophysiological and molecular techniques in transgenic mice. Nicotine intravenous self-administration (IVSA) was lower in constitutive β4 knockout (KO) mice at all doses tested (7.5, 15, 30 and 60 μg/kg/infusion) compared to wild-type (WT) mice. *In vivo* microdialysis showed that β4KO mice have higher extracellular dopamine (DA) levels in the nucleus accumbens than WT mice, and exhibit a differential sensitivity to nicotine-induced DA outflow. Furthermore, electrophysiological recordings in the ventral tegmental area (VTA) demonstrated that DA neurons of β4KO mice are sensitive to lower doses of nicotine than WT mice. Re-expression of β4* nAChRs in IPN neurons fully restored nicotine IVSA, and attenuated the increased sensitivity of VTA DA neurons to nicotine. These findings suggest that β4* nAChRs in the IPN play a role in maintaining nicotine IVSA.

INTRODUCTION

Tobacco is consumed by an estimated 1 billion people worldwide, and represents the primary cause of preventable morbidity and mortality, with 6 million deaths per year (World Health Organization, 2013). Nicotine is the principal psychoactive compound in tobacco, and stimulates the neurological reward system to drive its repeated intake. The maintenance of nicotine intake impedes cessation, and current therapies display weak support for abstinence (Hartmann-Boyce *et al*, 2013; Messer *et al*, 2008). It is therefore important to elucidate the neural mechanisms underlying nicotine addiction to aid in the development of an efficient smoking cessation therapy.

Nicotine exerts its effects by binding to nicotinic acetylcholine receptors (nAChRs). These transmembrane receptors are composed of alpha (α1-10) or alpha plus beta (β2-4) subunits, forming a diverse variety of homo- and hetero-pentameric ligand-gated ion channels endogenously activated by acetylcholine. Human genetic studies have highlighted the polymorphic nature of the *CHRNA5-CHRNA3-CHRNB4* genomic cluster, encoding subunits α5, α3 and β4, and its implication in smoking behaviors (Bierut *et al*, 2008). Furthermore, variants in the β4 regulatory domain reduce the age of tobacco initiation, whilst gain-of-function variants in *CHRNB4* reduce the risk of nicotine dependence (Haller *et al*, 2012; Saccone *et al*, 2009; Schlaepfer *et al*, 2008). Although cholinergic responses are unaffected in *CHRNB4* coding variants, nicotine-elicited currents are increased (Haller *et al*, 2012), which is reflected as aberrant nicotine aversion in mice expressing these variants (Slimak *et al*, 2014), and as fewer cigarettes smoked per day in humans (Haller *et al*, 2012). These studies have shown that the β4-containing (β4*) subpopulation of nAChRs merits further investigation.

The pharmacological properties of β4* nAChRs are distinct with respect to other nAChR subtypes, demonstrating lower sensitivity to nicotine compared to α4β2* nAChRs, and slower desensitization in the case of α3β4 (Fenster *et al*, 1997). Unlike the promiscuously expressed β2* nAChRs, β4* nAChRs demonstrate a discreet expression profile in the rodent central nervous system. The medial habenula (MHb) and interpeduncular nucleus (IPN) are the major hosts to β4* nAChRs (Salas *et al*, 2003). The

MHb receives input from the posterior septum (Yamaguchi *et al*, 2013), and sends neuronal efferents to co-release glutamate and acetylcholine onto GABAergic and serotonergic neurons of the IPN (Groenewegen *et al*, 1986; Ren *et al*, 2011). IPN neurons project to the raphe nucleus and dorsal tegmentum (Hsu *et al*, 2013), which provide neurological input to the ventral tegmental area (VTA) (Geisler and Zahm, 2005). Thus far, the MHb and IPN have been linked to anxiety, impulsivity, nicotine withdrawal, and primary reinforcement (Hsu *et al*, 2014; Kobayashi *et al*, 2013; Zhao-Shea *et al*, 2013).

The role of β4* nAChRs has been investigated in certain nicotine-mediated behaviors, including nicotine-elicited seizures (Salas et al., 2004), aversion (Frahm *et al*, 2011; Slimak *et al*, 2014), anxiety (Salas *et al*, 2003), and withdrawal (Salas *et al*, 2004; Zhao-Shea *et al*, 2013), supporting the involvement of this subunit in regulating the aversive properties of nicotine (Fowler and Kenny, 2013). However, recent findings provide evidence for their role in the habenulo-interpeduncular pathway in nicotine reinforcement. Notably, pharmacological inhibition of β4* nAChRs by local injection of the potent α3β4 nAChR antagonist, 18-MC in the MHb and the IPN modulated nicotine self-administration (Glick *et al*, 2011; Jackson *et al*, 2013), as well as nucleus accumbens (NAC) dopamine outflow stimulated by nicotine (McCallum et al., 2012) in rats.

In this study, we aimed to elucidate the role of β4* nAChRs in the MHb and IPN in a segregated manner. To do this, we used a combination of transgenic mouse lines, lentivirus technology, and assessment of nicotine-mediated behavioral and physiological outcomes. This allowed the establishment of the role of β4* nAChRs in the IPN independently of the β4-rich MHb.

MATERIALS AND METHODS

Mice

Experiments were conducted in male C57Bl/6J mice (wild-type, WT), and constitutive knockout (KO) mice lacking β4 nAChR subunits (Xu *et al*, 1999). β4KO mice were backcrossed onto a C57Bl/6J background for at least 20 generations. WT mice were not littermates but were matched for age and sex to the β4KO mice, and were bred in the same life conditions at Charles River (France). For the intravenous self-administration (IVSA) studies, mice (start age 8-14 weeks) were individually housed at Pompeu Fabra University in a temperature (21 ±1 ºC) and humidity (55 ±10%) controlled room in a reversed 12-h light/dark cycle (lights off 8.00 am). Experiments were performed during the dark phase of the reversed cycle. In the microdialysis experiments, a separate group of naïve male WT and β4KO were age-matched to the mice used in the IVSA studies (12-20 weeks old). Mice were individually housed in the animal facility at Pompeu Fabra University in a normal light/dark cycle (lights on 8:00 am), and experiments were carried out in the light phase of the cycle. In the electrophysiology experiments, male age-matched WT and β4KO mice (8-14 weeks old) were group-housed at UPMC facilities in a 12-h light/dark cycle, and experiments were carried out in the light phase of the cycle. For lentiviral injections, male WT and β4KO mice (8-14 weeks old) were group-housed at the Pasteur Institute in a 12-h light/dark cycle. A transgenic line housed at the Pasteur Institute, expressing cre-recombinase under a β4 promoter (provided by GENSAT) was back-crossed onto C57Bl/6J for at least 4 generations, then crossed onto a β4+/- background (β4+/-; Tg(Chrnb4-cre)OL57Gsat/+, herein β4cre. Male and female β4cre mice (8-16 weeks old) were used for histological characterization of β4-expressing neurons. This line was not viable on a β4-/- background. Genotyping was conducted by Transnetyx (Tennessee, USA). Food and water were available ad libitum, except during behavioral training. All procedures involving mice were ethically approved (European Communities Directive 86/60-EEC; Comitè Ètic d'Experimentació Animal-Parc de Recerca Biomèdica de Barcelona; Comité Éthique en Expérimentation Animale, Pasteur Institute, 2013-0097).

Drugs

(-)Nicotine hydrogen tartrate salt [(–)-1-methyl-2(3-pyridyl)pyrrolidine] (Sigma, Madrid, Spain) was dissolved in physiological saline (0.9%), and the pH adjusted to 7.4 with sodium hydroxide. Nicotine doses, reported as free base concentrations, were either contingently administered by intravenous route in the IVSA studies (0, 7.5, 15, 30, 60 μg/kg/infusion) and electrophysiological experiments (0, 5, 10, 15, 30, 60, 90 and 120 μg/kg) or by subcutaneous (s.c.) injection in the microdialysis experiments (0, 0.17, 0.24, 0.33 mg/kg).

Food maintained operant behavior and nicotine IVSA experiments

Behavioral experiments were conducted in mouse operant chambers (Model ENV-307A-CT; Med Associates Inc., Georgia, VT, USA) equipped with two nose-pokes, one randomly selected as the active nose-poke and the other as the inactive nose-poke. A cue light located above the active nose-poke (intensity of 20 mA) was paired contingently with the delivery of the reinforcer. Operant training was performed according to a previously described methodology with slight modifications (Orejarena et al., 2013). First, β4KO and WT controls were first trained to respond for standard food pellets (Testdiet, Richmond, IN, USA) on a fixed ratio (FR) 1 schedule of reinforcement until stable responding was obtained, and then on an FR3 schedule of reinforcement. An intra-jugular catheter was then implanted under anesthesia. After recovery from surgery, mice were re-trained on food responding and then trained to self-administer nicotine at the dose of 30 μg/kg/infusion during 10 days on an FR3 schedule of reinforcement. Subsequently, in β4KO and WT controls, a progressive ratio procedure was performed in order to test the motivation of the mice to work for nicotine at this dose, where the response requirement to earn an infusion escalated according to the following series: 1-2-3-5-12-18-27-40-60-90-135-200-300-450-675-1000, as previously described (Berrendero *et a.,* 2012). Further details regarding the operant training procedure are described in the Supplementary Information. Lentivirus-injected mice were submitted to the same food training procedure, 6 days of **nicotine** IVSA (30 μg/kg/infusion) but no progressive ratio schedule. Following stable responding, all mice underwent dose-response experiments as described previously (Orejarena et al., 2013), where nicotine doses were presented in the following

order: 7.5, 15, 30 and 60 µg/kg/infusion, with saline presented last. Each dose of nicotine was available during 3 consecutive days.

Viral expression vectors

The lentivirus vector used is based on the one previously described (Maskos *et al*, 2005), obtaining a bicistronic cassette that concomitantly expresses mouse β4 and GFP under a phosphoglycerate kinase promoter (PGK-β4). Control lentiviral vectors induced GFP expression only (PGK-GFP). Adeno-associated virus 2/1 serotype (pAAV.hSynap.Flex.GCaMP5G(GCaMP3-T302L.R303P.D380Y) WPRE.SV40, Vector Core, Pennsylvania) was used for histological analysis in order to indirectly identify and characterize β4-expressing neurons of the IPN without the masking effect of β4-rich MHb terminals. The AAV construct contains a synapsin promotor upstream of a GCaMP5 sequence flanked by loxP and loxP2272 sites, allowing expression of the fluorophore GCaMP5 in cre-recombinase expressing cells only.

Stereotaxic delivery of lentiviral vector

Stereotaxic delivery of viruses to WT and KO mice was performed as previously described (Tolu *et al*, 2013) with the following modifications. The MHb was targeted from bregma and skull surface at: anterior: -1.70 and -1.90 mm, lateral: ±1.25 mm and ventral: -2.40 mm (Paxinos and Franklin, 2004). Injections were conducted using pulled glass pipettes at an angle of ± 20°. Two 0.5 µl volumes of lentivirus were delivered bilaterally at 0.2 µl/min (PGK-β4 300 ng/µl, PGK-GFP 75 ng/µl p24 protein). The IPN was targeted at anterior: -3.60 mm, lateral: -1.60 mm and ventral -4.50 mm to bregma and skull surface at an angle of -20° (Paxinos *et al*, 2004). A metal 35-gauge needle was used to deliver a single injection of 2 µl lentivirus to the central region of the IPN (PGK-β4 75 ng/µl, PGK-GFP 25 ng/µl p24 protein), or 0.5-1.0 µl (10^{11} GC) of AAV. Lentivirus-injected mice underwent behavioral or electrophysiological testing 4 weeks post-injection. AAV-injected mice were sacrificed 2-4 weeks post-injection for immunohistological analysis.

Verification and quantification of β4* expression in the MHb and IPN

For radioligand binding preparation, lentivirus-injected mice were euthanized by cervical dislocation at the end of the IVSA experiments. Fresh brains were frozen to -80°C, and coronal sections (20 µm) were

thaw-mounted onto Superfrost microscope slides. *In situ* autoradiography was conducted as previously reported (Frahm *et al*, 2011) with the use of 25 nM 5-Iodo-A-85380 dihydrochloride (5-I-A85380, Tocris Bioscience, Bristol UK) as the cold ligand for displacement of 220 pM I^{125}-epibatidine (2200Ci/mmol specific activity, PerkinElmer, Inc., Waltham MA) from β2* nAChR sites. Once dry, slides were exposed to a Kodak MR film for 16 h, developed (Kodak X-OMAT 2000), and the film scanned at 1600 dpi. Total I^{125}-epibatidine binding localizes heteromeric (β2* and β4*) nAChRs. 5-I-A85380 displaces I^{125}-epibatidine from β2* nAChR sites, allowing us to localize and quantify expression of putatively β4* nAChRs. The 5-I-A85380-resistant I^{125}-epibatidine images were used for quantification using Image J (1/luminosity minus mean background over 3 points). Slides were stained with 0.1% Cresyl violet and progressively dehydrated in 50-100% EtOH and histoclear. We verified that slices were intact and that the autoradiographic punctua corresponded to the targeted brain region. Each MHb is considered as independent, giving n=2 per brain. The IPN is quantified as a single entity, giving n=1 per brain.

Immunofluorescence

Immunofluorescence studies were carried out at the end of behavioral and electrophysiological testing in mice injected with lentivirus, and in mice injected with AAV not submitted to any experimental procedure. Mice were deeply anaesthetized with a ketamine:xylazine solution (5:1; 0.10 ml/10 g) via intraperitoneal (i.p.) route and perfused intracardially with PBS and 4% PFA. Coronal brain slices of 60 μm thickness were obtained using a vibratome (Leica Microsystems, Wetzlar, Germany) and incubated in 10% normal horse serum (NHS) and 0.2% triton-X in PBS for 4 h. Antibody labeling was conducted in 2% NHS and 0.04% triton-X solution. Primary antibodies used: rabbit anti-GFP (Life Technology, OR USA), sheep anti-tyrosine hydroxylase (Millipore, CA USA), goat anti-choline acetyl Transferase (Chemicon, CA USA), goat anti-somatostatin (Santa Cruz Biotechnology, CA), at a 1:500 dilution, overnight, 4°C. Sections were rinsed and secondary antibody labeling conducted at a 1:500 dilution, 4 h, room temperature. Antibodies used: Alexa-488 donkey anti-rabbit (Abcam), Alexa-546 donkey anti-goat (Life Technologies), Cy5 donkey anti-sheep (Jackson). Images were taken using a Zeiss fluorescent microscope. Colocalization was quantified using Image J software.

Microdialysis experiments

A separate group of naïve male β4KO and WT mice were anesthetized with a ketamine:xylazine (5:1; 0.10 ml/10 g, i.p.) solution and placed in a stereotaxic apparatus. Unilateral microdialysis probes (CMA7: 1 mm, CMA Microdialysis, Stockholm, Sweden) were directly implanted vertically in the NAC (anterior +1.5; ±0.8 lateral; ventral -4.8 mm) from bregma and skull surface according to the coordinates of Paxinos and Franklin (2004), and then fixed to the skull with dental cement. Two days after surgery, mice were habituated to the microdialysis environment overnight. The following morning, probes were perfused with a ringer solution (NaCl: 148 mM, KCl: 2.7 mM, CaCl2:1.2 mM and MgCl2: 0.8 mM, pH 6.0) at a constant rate of 1 µl/min during 1 h (see supplementary information). Subsequently, 4 dialysates were collected in each mouse in order to determine baseline DA efflux. Then, separate groups of mice were challenged first with saline followed by one dose of nicotine (0.17, 0.24 or 0.33 mg/kg, s.c.). Four samples were collected after saline and 8 samples after nicotine administration at 15 minute intervals.

Electrophysiology experiments

A separate group of naïve β4KO and WT mice were anaesthetized with chloral hydrate (8%), 400 mg/kg (i.p.), and positioned in a stereotaxic frame with a catheter inserted into the mouse's saphenous vein for intravenous administration of drugs. Body temperature was maintained at 37°C. Glass recording electrodes (tip diameter of 1-2 mm and impedance of 4-8 MΩ) were placed in the VTA: anterior -2.90 to -3.9 mm, lateral ±0.24 to ±0.96 mm, and ventral -3.5 to -4.5mm from bregma and skull surface (Paxinos *et al*, 2004). Extracellular identification of dopamine (DA) neurons was based on their location as well as on the set of unique electrophysiological properties that characterize these cells *in vivo* (Ungless and Grace, 2012). Baseline recordings were conducted during 10-20 min followed by and injection of 10 µl of saline (i.v.), and recordings were performed again for 5-10 min. Subsequently, nicotine (5, 10, 15, 30, 60, 90 and 120 µg/kg; i.v.) was injected in a random sequence, with a delay of 15-30 min between consecutive injections. Recordings from a single DA neuron were conducted after one to four injections of nicotine at different doses. DA cell firing was analyzed with respect to the average firing rate and the percentage of spikes within a burst, as previously described (Morel *et al*, 2014). To quantify nicotine effects, the maximum of fluctuation on a 3-min period after injection was determined. Lentiviral-injected β4KO mice for

electrophysiological studies came from the Pasteur Institute breeding facilities. See Supp. Fig. 1 for a schematic representation of the experimental procedures stating ages, numbers and sources of mice, as well as the order, duration and location of experiments.

Statistical Analysis

The food and nicotine **IVSA** data were analyzed using two- or three-way repeated measures ANOVA (Statistical Package for the Social Sciences, SPSS and GraphPad Prism 6) with days and nose-poke (active-inactive) responding as intra-subject factors and genotype as a between subject factor, followed by estimation of parameters or LSD post-hoc tests. The nicotine dose-response data (infusions) were analyzed by two-way repeated measures ANOVA with dose as an intra-subject factor and genotype as a between subject factor, followed by LSD post-hoc test. Statistical analysis of nicotine intake (μg/kg) was performed using one-way ANOVA with Tukey's post-hoc test. For the microdialysis experiments, the changes in DA levels (percent of baseline) for each dose of nicotine and saline were analyzed separately using a two-way repeated measures ANOVA comparing between genotypes, the mean of 4 baseline dialysates to each of 8 dialysates following nicotine administration, followed by the LSD post-hoc test. Analysis of autoradiographic data was performed using unpaired t-tests or Welch two-sample t-test if variances were not equal. For electrophysiology studies, the minimum dose necessary to activate DA cells was determined. Changes in firing frequency were analyzed using one-way ANOVA, and t-tests were used to determine significant group effects and deviations from saline responses. When the variance of the two samples was not equal in the t-tests, a Welch (or Satterthwaite) approximation of the degrees of freedom was used. Changes in the proportion of spikes within bursts (SWB) were analyzed using the Kruskal-Wallis test, and the Wilcoxon test was used to determine significant group effects and deviations from saline.

RESULTS

Food maintained operant behavior is similar in β4KO and WT mice

β4KO and WT mice from two batches were first trained to respond for food reward, and the data pooled together. The number of pellets earned on an FR1 schedule of reinforcement by 41 WT and 36 β4KO mice is shown on Fig. 1A. A significant effect of training day ($F(7,525)=97.8$, $p<0.001$), but no significant effects of genotype or interaction between factors were revealed. On the FR3 reinforcement schedule, a significant effect of day ($F(5,375)=9.3$, $p<0.001$), but no genotype effect or interaction between factors were observed. 3 WT and 9 β4KO did not survive catheter surgery. The remaining mice (WT n=38, β4KO n=27) were retrained on an FR3 reinforcement schedule for food reward during 3 days. A significant effect of day ($F(2,126)=15.5$, $p<0.001$), but no genotype effect or interaction between factors were observed. These results indicate that β4KO mice learn an operant reinforced behavior in a similar manner to WT mice. Nose-poke responses during food **training** are described in the supplementary results and Supp. Fig. 2A

β4KO mice show deficits in nicotine IVSA on an FR3 schedule of reinforcement and the progressive ratio procedure

Following food retraining, the remaining mice (WT n=38, β4KO n=27) were trained on **IVSA of nicotine** at the dose of 30 μg/kg/infusion on an FR3 schedule of reinforcement. 16 WT and 12 KO mice did not complete this phase due to problems with catheter patency or death due to illness. **Stable responding for nicotine was determined according to the following criteria:** 1) less than 20% deviation from the mean of the total number of reinforcers during 3 consecutive days, 2) at least 65% responding on the active nose-poke, and 3) a minimum of five reinforcers per session. More WT (77.27%) than KO mice (13.33%) **achieved these criteria** during the10 days of training. Statistical analysis showed that β4KO mice earned a significantly lower number of nicotine infusions with respect to WT mice at this dose (genotype, $F(1,35)=8.5$, $p<0.01$; day ($F(9,315)=2.2$, $p<0.05$), but no significant interaction between factors were observed (Fig. 1B). Furthermore, a significant decrease in the area under the curve (AUC) for β4KO mice was revealed ($F(1,36)=8.8$, $p<0.01$) compared to WT mice (Fig. 1B inset). Nose-poke responses **during**

nicotine IVSA training are described in the supplementary results and Supp. Fig. 2B. **Mice were then submitted to** a progressive schedule of reinforcement (Fig. 1C). A significant decrease in breaking point (BP) was revealed for β4KO mice (mean ± S.E.M. BP: 4.0 ± 1.3; mean ± S.E.M number of infusions: 2.6 ± 0.5; as compared to WT mice (mean ± S.E.M BP: 12.4 ± 2.5; mean ± S.E.M number of infusions: 4.5 ± 0.4) $F(1,36)=6.9$, $p<0.05$), indicating less motivation to work for the drug. Since the ratio of responding required to obtain a nicotine infusion increases rapidly, the difference in active responding required to earn 4.5 ± 0.4 and 2.6 ± 0.47 infusions is quite substantial (mean ± S.E.M active nose-pokes WT: 38.2 ± 9.7 vs. mean ± S.E.M active nose-pokes KO: 10.4 ± 3.8).

β4KO mice show alterations in nicotine IVSA dose-response

Subsequently, mice (WT n=22, β4KO n=15) were assessed in a dose-response curve (Fig. 1D). 11 WT and 6 KO mice did not complete this phase due to problems with catheter patency. For mice that completed this procedure (WT n=11, β4KO n=9), significant effects of dose ($F(4,72)=16.7$, $p<0.001$), genotype ($F(1,18)=74.5$, $p<0.01$), and interaction between factors were observed ($F(4,72)=4.4$, $p<0.01$). Post-hoc comparisons revealed that WT mice self-administered significantly more nicotine than saline at the doses of 7.5, 15 and 30 μg/kg/infusion ($p<0.001$). β4KO mice showed significantly more nicotine intake than saline at the doses of 7.5 and 15 μg/kg/infusion ($p<0.01$). Notably, β4KO mice self-administered less nicotine than WT mice at all the doses tested except saline (7.5, 30.0 and 60.0 μg/kg/infusion, $p<0.01$; 15 μg/kg/infusion, $p<0.05$). The mice that completed this procedure showed no difference in their operant responding for food reward and **nicotine IVSA at the dose of 30 μg/kg/infusion, prior to the nicotine dose-response assessment** with respect to the pooled data shown in Fig. 1 A-C.

β4KO mice demonstrate basal NAC hyperdopaminergia and dysregulated nicotine-induced increase in NAC DA outflow

Basal extracellular levels of DA in the NAC were significantly higher in naïve β4KO mice (4.01 ± 0.32 pg/15 μl) than in WT controls (2.61 ± 0.19 pg/15 μl, genotype effect: $F(1,24)=6.4$, $p<0.05$; Fig. 2A). A challenge injection of saline did not change the levels of DA with respect to baseline in either group (WT =

2.37 ± 0.26 pg/15 µl, KO = 3.61 ± 0.47 pg/15 µl, Fig. 2A). The acute administration of 0.17 mg/kg nicotine did not significantly modify DA extracellular levels at any time point in either group (Fig. 2B). A significant increase in DA outflow in the NAC was observed with 0.24 mg/kg nicotine with respect to baseline in β4KO, but not in WT mice (Fig. 2C; time effect, $F(8,64)=5.6$, $p<0.001$; interaction between factors, $F(8,64)=2.5$, $p<0.05$). Post-hoc analysis showed significant differences between genotypes 15, 75 and 90 min after nicotine administration ($p<0.05$). In contrast, at 0.33 mg/kg nicotine, DA outflow increased in WT but not in KO mice (Fig. 2D; time effect, $F(8,88)=15.9$, $p<0.001$; interaction between factors, $F(8,88)=3.0$, $p<0.01$). Post-hoc analysis showed significant differences between genotypes 15 min after nicotine administration only ($p<0.05$).

VTA DAergic neurons of β4KO mice demonstrate an increased sensitivity to nicotine.

We performed *in vivo* electrophysiological recordings in naïve WT and β4KO mice in order to address the role of the β4* nAChRs in VTA DA cells' response to nicotine. No differences were observed in the spontaneous activity of DA cells in WT (2.8 ± 0.2 Hz) and β4KO (2.6 ± 0.2 Hz) mice, nor in the percentage of spikes within bursts (WT: 12.3 ± 2.2, KO: 13.4 ± 2.0) (Fig. 3A). One-way ANOVA demonstrated a dose effect on firing frequency in WT ($F(5,152)=8.8$, $p<0.001$) and a tendency in β4KO mice ($F(5,119)=2.1$, $p=0.06$). A t-test comparing saline to pooled nicotinic responses showed that there is indeed a response to nicotine ($t=-3.5$, $df=83.2$, $p<0.001$). Subsequent t-tests comparing firing frequency responses between each dose and saline demonstrated that VTA DAergic neurons of β4KO mice are more sensitive to nicotine-evoked changes in firing frequency than WT mice. 15 µg/kg nicotine was sufficient to increase DA cell firing frequency in WT DA neurons ($t=-2.8$, $df=9.2$, $p<0.05$), whereas 5 µg/kg nicotine was sufficient to increase DA neuron firing frequency of β4KO mice ($t=-2.5$, $df=12.6$, $p<0.05$, Fig. 3B). Furthermore, the evoked responses were significantly higher in β4KO mice than in WT following administration of 10 µg/kg nicotine (ΔFrequency, $t=-3.3$, $df=16.2$, $p<0.01$; Δ%SWB, $W=23$, $p<0.05$). Kruskal-Wallis analysis of nicotine-evoked changes in the proportion of spikes within bursts revealed a significant dose-effect in WT ($X^2=13.5$, $df=5$, $p<0.05$), but not β4KO VTA DA responses to nicotine (Fig. 3C). Due to an insufficient number of recordings, responses to 90 and 120 µg/kg nicotine are not presented.

Re-expression of β4* nAChRs in the MHb

A lentivirus was generated for re-expression of β4 nAChR subunits in brain regions of interest (Fig. 4A). *In situ* autoradiography revealed the MHb and IPN as major hosts of β4* nAChR expression in WT mice, and that 5-I-A85380-resistant I^{125}-epibatidine binding was reduced in both structures of β4KO mice (Fig. 4B). Residual binding was observed in the MHb of nicotine-exposed PGK-GFP-injected KO mice (KO-GFP^{MHb}, 11.7 ± 3.6 %, Fig. 4B, Fig. 5A inset). PGK-β4 lentivirus injections to the MHb and IPN of KO mice (KO-$\beta4^{MHb}$, KO-$\beta4^{IPN}$, respectively) resulted in restoration of radioligand-binding sites, demonstrating that exogenous β4 subunits are able to assemble with endogenous nAChR subunit partners to form the obligatory inter-subunit epibatidine binding site (Fig. 4B; Hansen *et al*, 2005). GFP fluorescence demonstrated that the majority of the MHb was infected and that these neurons project to the IPN (Fig. 4D, Supp. Fig. 3A). Viral GFP in the terminals co-localizes with the cholinergic marker anti-choline acetyl transferase (ChAT), and extends to the ChAT-negative lateral IPN (Supp. Fig. 3A). Virally induced expression of MHb β4 also rescues β4* nAChR expression in the terminals supplying the IPN (Supp. Fig. 3B).

Autoradiographic analysis of KO-$\beta4^{MHb}$ brains following nicotine IVSA revealed the heterogenous nature of β4 re-expression amongst individuals. Therefore, we performed a qualitative correlation assessment between levels of β4* re-expression and nicotine IVSA, where a threshold effect of β4* nAChRs expression on behavior was observed. KO-$\beta4^{MHb}$ mice were subdivided into two groups depending on the extent of β4* nAChRs re-expression, and those with KO-like 5-I-A85380-resistant I^{125}-epibatidine binding removed from the data. One group of KO-$\beta4^{MHb}$ (*low expressers*), whilst showing statistically significant re-expression of β4* nAChRs (26.0% ± 3.6%, $p<0.01$ compared to KO-GFP^{MHb}, Supp. Fig. 2E inset), showed no rescue of nicotine IVSA at any of the nicotine doses tested (see Supp. Information, Supp Fig. 2E). The data for a second group of KO-$\beta4^{MHb}$ mice showing greater β4* nAChRs re-expression (58.6% ± 8.4%, $p<0.01$ compared to KO-GFP^{MHb}, Fig. 5A inset) are described below.

Partial re-expression of β4* nAChRs in the MHb does not fully rescue nicotine IVSA

WT mice were injected with a control lentivirus (WT-GFP^{MHb}), and β4KO mice were injected with either a control lentivirus (KO-GFP^{MHb}) or a PGK-β4 lentivirus (KO-β4^{MHb}, Fig. 4B and 4D) in the MHb. Following catheter surgery, mice were re-trained on food maintained operant behavior. No significant differences between genotypes were observed in this task (mean number of pellets obtained in 1 h by WT-GFP^{MHb}: 68.81 ± 6.89; KO-GFP^{MHb}: 49.13 ± 6.42; KO-β4^{MHb}:50.0 ± 6.14). Subsequently, mice were trained to acquire nicotine IVSA at the dose of 30 µg/kg/infusion on an FR3 schedule of reinforcement (see Supp. Information, Supp. Fig 2C). Next, a dose-response curve was determined. The number of infusions earned for the various doses of nicotine by WT-GFP^{MHb}, KO-GFP^{MHb} and KO-β4^{MHb} mice is shown in Fig. 5A. A significant group ($F(2, 21)=6.1$, $p<0.01$) and dose effect ($F(4, 84)=27.3$, $p<0.0001$), but no significant interaction between factors was revealed. The mean nicotine intake is shown on Fig. 5B. KO-GFP^{MHb} consumed less nicotine than WT-GFP^{MHb} at the doses of 15.0 ($F(2,20)=6.2$, $p<0.01$) and 30.0 µg/kg/infusion ($F(2,20)=4.7$, $p<0.05$). KO-β4^{MHb} mice consumed an intermediate amount of nicotine at all nicotine doses, with no statistical differences compared to WT-GFP^{MHb} or KO-GFP^{MHb} mice.

Re-expression of β4* nAChRs in the IPN rescues nicotine IVSA

β4cre mice, expressing cre-recombinase under a β4 promoter, were injected with an AAV in the IPN for conditional expression of the fluorophore GCaMP5 (Fig. 4C). Immunohistofluorescence analyses revealed that these neurons co-localize with somatostatin immunoreactivity (95%, Supp. Fig. 3E and 3F). β4cre neurons occupy the dorsal part of the anterior IPN at positions -3.3 to -3.5 mm from bregma, and progressively invade the more ventral portion of the IPN towards -3.8 mm from bregma (n=5). No fluorescence was detected in IPN target structures including the laterodorsal tegmentum or raphe nuclei.

WT mice were injected in the IPN with a control lentivirus (WT-GFP^{IPN}) and β4KO mice with control (KO-GFP^{IPN}) or PGK-β4 lentivirus (KO-β4^{IPN}). Infection of somatostatin-positive IPN neurons by the PGK-β4 lentivirus was verified (Supp. Fig. 3G). The role of β4 on neurons of the IPN in nicotine IVSA was investigated. GFP fluorescence and 5-I-A85380-resistant I^{125}-epibatidine binding was detected in the IPN

and the laterodorsal tegmentum (Supp. Fig. 3C, and 3D). Assessment of radioligand binding was conducted in all but two KO-β4^{IPN} brains. On-target β4* nAChR re-expression was observed in all brains assessed (KO-β4^{IPN} 63.7%, ± 11.8%; KO-GFP^{IPN} 1.3%, ± 0.8%; Fig. 5C inset). All mice were therefore included in the behavioral data.

Following catheter surgery, mice were re-trained on food maintained operant behavior. No significant differences between genotypes were observed in this task (mean number of pellets obtained in 1 h by WT-GFP^{IPN}, 36.9 ± 3.5; KO-GFP^{IPN}, 31.3 ± 2.3; KO-β4^{IPN}, 30.7 ± 4.0). Subsequently, mice were trained to acquire nicotine IVSA at the dose of 30 µg/kg/infusion on an FR3 reinforcement schedule (see Supplementary information, Supp. Fig 2D). Next, a dose-response curve was determined (Fig. 5C). For the number of infusions earned, a significant effect of group ($F(2, 21)=10.2$, $p<0.001$), dose ($F(4, 84)=26.6$, $p<0.001$), and interaction between factors ($F(8, 84)=5.4$, $p<0.001$) was observed. Post-hoc analysis revealed that KO-GFP^{IPN} self-administered significantly less nicotine than WT-GFP^{IPN} at the doses of 7.5, 15 and 30 µg/kg/infusion ($p<0.001$). In KO-β4^{IPN} mice, self-administration of nicotine was restored to WT-GFP^{IPN} levels at the doses of 7.5 and 15.0 µg/kg/infusion, but not at the dose of 30 µg/kg/infusion, where they self-administered significantly more nicotine than KO-GFP^{IPN} ($p<0.05$), but less than WT-GFP^{IPN} ($p<0.05$) mice. No statistical differences between groups were observed with IVSA of saline or 60 µg/kg/infusion of nicotine. This was reflected in the nicotine consumed (Fig. 5D), where KO-β4^{IPN} mice consumed more nicotine than KO-GFP^{IPN} at the doses of 7.5 and 15.0 µg/kg/infusion. However, at 30 and 60 µg/kg/infusion, KO-β4^{IPN} showed no significant differences to KO-GFP^{IPN} or WT-GFP^{IPN} mice.

Re-expression of β4* nAChRs in the IPN rescues VTA DAergic responses to nicotine

VTA DA analysis in KO mice revealed a difference in the nicotine-evoked responses at the dose of 10 µg/kg. *In vivo* VTA DAergic electrophysiological responses to 0, 10 and 30 µg/kg were thus investigated in WT-GFP^{IPN}, KO-GFP^{IPN} and KO-β4^{IPN} mice, first to confirm previous results and then to estimate the

effect of re-expression. WT-GFP^{IPN} mice showed an increase in firing frequency ($t=-4.1$, $df=26.1$, $p<0.001$), and in the proportion of spikes within bursts ($W=278.5$, $p<0.05$) following i.v. injection of 30 μg/kg nicotine but not 10 μg/kg nicotine (Fig. 5E, 5F). KO-GFP^{IPN} mice showed an increase in sensitivity to nicotine-evoked increases in DA cell activity relative to saline, confirming findings in WT and β4KO mice (Fig. 3). The firing frequency and proportion of spikes within bursts was increased at the dose of 10 μg/kg ($t=-3.8$, $df=11.8$, $p<0.01$; $W=53$, $p<0.01$, respectively), and at the dose of 30 μg/kg ($t=-2.8$, $df=18.4$, $p<0.05$; $W=123$, $p<0.05$, respectively). Responses in KO-β4^{IPN} mice were restored to the WT-GFP^{IPN}-like phenotype, with an increase in nicotine-evoked firing frequency at the dose of 30 μg/kg ($t=-2.2$, $df=13.7$, $p<0.05$), but not at 10 μg/kg nicotine. Firing frequency responses in WT-GFP^{IPN} mice were similar to those of KO-β4^{IPN}, but different to KO-GFP^{IPN} (WT-GFP^{IPN} versus KO-GFP^{IPN}, $t=-3.0$, $df=11.6$, $p<0.05$; KO-β4 versus KO-GFP^{IPN}, $t=2.6$, $df=13.9$, $p<0.05$). The proportion of spikes within bursts was increased in KO-β4^{IPN} mice at the dose of 10 ($W=30$, $p<0.05$), but not at 30 μg/kg nicotine relative to saline. The proportion of spikes within bursts in KO-β4^{IPN} mice were similar to those of WT-GFP^{IPN}, but different to KO-GFP^{IPN} (WT-GFP^{IPN} versus KO-GFP^{IPN}, $W=114.5$, $p<0.01$; KO-β4^{IPN} versus KO-GFP^{IPN}, $W=35.5$, $p<0.01$).

DISCUSSION

Several recent human genetic studies have highlighted the polymorphic nature of the *CHRNA5-CHRNA3-CHRNB4* gene cluster, and its contribution to smoking behaviors and dependence risk. Notably, variants in *CHRNB4*'s coding region reduce the risk for nicotine dependence (Haller *et al*, 2012), and variants in *CHRNB4*'s regulatory domain decrease the age of onset for tobacco **intake** (Schlaepfer *et al*, 2008). The present study aimed to elucidate the role of β4* nAChRs in nicotine reinforcement in mice, and the underpinning physiological correlates.

For this purpose, we first evaluated operant nicotine IVSA behavior in WT and β4KO mice. This experimental procedure has been shown to be a reliable method to model in mice the addictive potential of several drugs of abuse, including nicotine (Orejarena *et al*, 2012; Sanchis-Segura and Spanagel, 2006). This procedure incorporates various aspects of human smoking behaviors such as the volitional aspects, rapid nicotine delivery via systemic route, and chronic exposure to the drug. β4KO mice show decreased nicotine IVSA at all doses tested (7.5, 15, 30 and 60 μg/kg/infusion) as compared to WT controls, as well as a decrease in motivation to self-administer nicotine. This is not due to cognitive deficits since WT and β4KO mice alike self-administer food successfully during operant training.

These results showing that the lack of β4* nAChR reduces the reinforcing properties of nicotine can be contrasted with other studies using transgenic mice overexpressing Chrnb4 exhibiting a strong aversion to nicotine (Frahm et al, 2011). These divergent data highlight the balance of positive and aversive signaling mechanisms associated with nicotine intake, which can be revealed using different paradigms in mice. In the Frahm study, the aversive properties of nicotine were demonstrated with the conditioned place aversion and the two-bottle choice tests, **while in our study we used an IVSA procedure with lower doses of nicotine to determine the overall reinforcing effects of the drug.** In line with our findings showing that β4* nAChR contribute to the reinforcing properties of nicotine, a recent study demonstrated that inhibiting cerebral β4* nAChRs with the selective α3β4* nAChR antagonist, α-conotoxin AuIB, attenuates nicotine-conditioned place preference in C57BL/6J mice (Jackson et al., 2013).

Potential underlying neural mechanisms were explored in order to elucidate the physiological correlates resolving the nicotine self-administration deficit. The mesolimbic DA system is an established substrate for the rewarding properties of nicotine (Di Chiara *et al*, 2004). Therefore, we investigated whether the β4KO's behavioral deficit was reflected in the mesolimbic DA response to nicotine *in vivo* with neural networks intact, including the β4* nAChR-enriched habenulo-interpeduncular pathway. Microdialysis experiments in the NAC revealed higher basal extracellular levels of DA in β4KO versus WT mice. A reinforcing dose of nicotine (0.33 mg/kg; Walters *et al*, 2006) was effective in eliciting an increase in NAC DA outflow in WT controls mice, but not in β4KO mice. These results are consistent with previous data showing that conditioned place preference induced by a rewarding dose of nicotine is blunted by intracerebroventricular blockade of β4* nAChRs (Jackson *et al*, 2013), known to depend upon intact mesolimbic responses (Fields *et al*, 2007). Unexpectedly, a sub-effective dose of nicotine in WT mice (0.24 mg/kg) induced an increase in DA extracellular levels in the NAC of β4KO mice, indicating a differential sensitivity to nicotine-induced DA outflow in these mice with respect to WT mice. Basal responding was unaltered in *in vivo* electrophysiological assessment of VTA DAergic neurons of β4KO mice; however these neurons demonstrated an increase in sensitivity to acute doses of nicotine. This altered sensitivity to nicotine may be facilitating the downward shift of the dose-response curve in the nicotine IVSA procedure, although it remains to be determined whether these responses represent those occurring during nicotine IVSA. This idea is in agreement with a previous study showing that enhancing DA activity in the NAC core increased satiety-like responses to intravenously self-administered cocaine (Suto and Wise, 2011). All together, these data indicate that β4* nAChRs regulate dopaminergic activity in the VTA and NAC, and modulate the reinforcing properties of nicotine.

β4* nAChR are mainly located in the habenulo-interpeduncular pathway (Salas *et al*, 2003). In order to understand the role of β4* nAChR in a region-specific manner, we undertook a stratified analysis by selectively re-expressing β4* nAChR in the MHb and the IPN of β4KO mice, and determining the reinforcing effects of nicotine. Lentivirus-mediated gene delivery to the MHb restored β4 nAChR subunit expression on a β4KO background, forming putative α3β4* nAChRs in MHb soma and terminals

innervating the IPN. MHb β4* nAChRs are required for nicotine-evoked excitatory responses (Dao *et al*, 2014; Görlich *et al*, 2013; Hsu *et al*, 2013), and β4* nAChRs on MHb terminals are required for nicotine-evoked acetylcholine release (Beiranvand *et al*, 2014; Grady *et al*, 2009). We found that partial re-expression of β4* nAChRs along the length of MHb neurons (mean: 26.0%) did not rescue nicotine IVSA. Those with higher (mean: 58.6%) re-expression levels consumed nicotine at intermediate amounts compared to WT-GFP^{MHb} and KO-GFP^{MHb} mice. Thus, it is possible that greater levels of β4* re-expression in the MHb are needed to completely restore nicotine reinforcing properties. **We also cannot rule out the effect of ectopic expression of β4* nAChRs in neuronal subpopulations of the targeted brain region, and of viral infection in the portion of the dorsal hippocampus adjacent to the dorsal third ventricle.** It is interesting to consider this finding in the context of human genetic studies: a variant in *CHRNB4*'s 3' untranslated region reduces the age of onset of habitual smoking (Schlaepfer *et al*, 2008) and alters gene expression (Gallego *et al*, 2013), a known limiting factor for α3β4 receptor activity (Frahm *et al*, 2011).

Conditional expression of a fluorophore in β4-expressing IPN neurons allowed visualization of β4 subunit expression without the masking effects of β4 from MHb terminals. This strategy located β4 expression to the dorsal portion of the IPN, with colocalization to somatostatin-positive interneurons. Re-expressing β4* on IPN neurons fully rescued self-administration of nicotine at the doses of 7.5 and 15.0 μg/kg/infusion. This also restored the deficit in VTA DAergic responses to nicotine, as determined by *in vivo* electrophysiology. This suggests that β4* nAChRs in the IPN regulate VTA DAergic responses to nicotine, and may be responsible for the observed restoration of nicotine IVSA. These findings diverge from previous studies in rats where local blockade of β4* nAChRs by the α3β4 nAChR antagonist, 18-MC in the MHb and the IPN decreased and increased nicotine IVSA respectively (Glick et al, 2011), suggesting an opposite role for β4* in these two structures in nicotine reinforcement. Furthermore, these authors found that local inhibition of β4* nAChRs with 18-MC in the MHb prevented the increase in NAC DA stimulated by nicotine in rats, whilst 18-MC application in the IPN increased the response (McCallum et al., 2012). However, since only one dose of nicotine was tested in the IVSA study (28 μg/kg/infusion), and microdialysis study (0.4 mg/kg, s.c.), the question remains as to whether these effects are pertinent to

other doses.

The present study corroborates the involvement of the habenulo-interpeduncular pathway in nicotine intake (Tuesta *et al*, 2011; Frahm *et al*, 2011). Furthermore, recent work has revealed that α5 nAChRs located in the MHb play a role in regulating the aversive properties of nicotine (Fowler *et al*., 2011). In addition, it has been shown that the balanced influence of α5 and β4 subunits in the MHb is critical for this function since transgenic mice overexpressing β4* nAChRs exhibit a strong aversion to nicotine that can be reduced by expression of an α5 loss-of-function variant in the MHb (Frahm *et al*, 2011). It is therefore possible that a constellation of expression- and function-altering variants in the *CHRNA5-CHRNA3-CHRNB4* gene cluster contribute to human smoking behaviors.

In summary, by using a stratified approach to investigate β4* nAChR function, we have demonstrated for the first time that these receptors located post-synaptically in the IPN are critical for nicotine reinforcement, and do not exclusively modulate nicotine aversion and withdrawal, as has been reported previously (Salas *et al*, 2009; Zhao-Shea *et al*, 2013). We also provide evidence for the role of β4* nAChRs in the IPN for modulating meso-accumbal DA responses to nicotine. Restoring IPN β4* nAChR expression, whilst not rescuing MHb cholinergic input, would allow direct nicotinic activation of the structure. With a lack of direct innervation of the IPN to the VTA (Antolin-Fontes *et al*, 2014), systemic nicotine acting at IPN β4* nAChRs presumably engages indirect pathways that regulate dopaminergic activity in the VTA such as the dorsal raphe nucleus, laterodorsal tegmentum or pedunculopontine tegmentum (Antolin-Fontes *et al*, 2014).

FUNDING AND DISCLOSURE

The authors declare no conflict of interest.

ACKNOWLEDGMENTS

This work was supported by the Spanish Instituto de Salud Carlos III (RD06/001/001 and PI10/01708), FEDER funds, and Ministerio de Ciencia e Innovación (#SAF2014-59648-P), the Catalan Government AGAUR (#2014-SGR-1547), Plan Nacional Sobre Drogas, Ministerio de Sanidad, Asuntos Sociales e Igualdad-MSASI (#PNSD-2013-0068), and FP7 ERANET program (NICO-GENE), the ICREA Foundation (ICREA Academia-2008), and a post-doctoral fellowship from CONACyT to AHS. Work in Paris was supported by the Institut Pasteur, Centre National de la Recherche Scientifique CNRS UMR 3571, the Agence Nationale pour la Recherche (ANR Neuroscience), and FP7 ERANET program (NICO-GENE), Grant agreement n009 BLANC 20092009BLANC 20 *NeuroCypres*" project), the École des Neurosciences de Paris (ENP), Fondation EDF, and the Fondation des Treilles.

We would like to thank Martine Soudant, Stephanie Pons and Dulce Real for technical support, and Inés Ibañes-Tallon and Jessica Ables for providing the Tg(Chrnb4-cre)OL57Gsat/+ transgenic mice.

FIGURE LEGENDS

Figure 1. Operant responding for food pellets and intravenous nicotine in WT and β4KO mice. A) Food pellets earned on an FR1 schedule of reinforcement during 8 days followed by an FR3 during 6 days in WT (n=41) and β4KO (n=36) mice, and 3 days of re-training after catheter surgery (WT n=38, β4KO n=27). Results are expressed as mean number of food pellets in 1 h ± S.E.M. B) Nicotine IVSA in WT (n=22) and β4KO (n=15) mice. Mice were trained on an FR3 schedule of reinforcement during 10 days to respond for nicotine at a dose of 30 μg/kg/infusion. Results are expressed as mean number nicotine infusions in 1 h ± S.E.M. Two-way repeated measures ANOVA, **p<0.01 genotype effect. The inset shows the area under the curve for active nose-poke responding in WT and β4KO mice (**p<0.01 WT vs. KO). C) Progressive ratio schedule of reinforcement in WT (n=22) and β4KO (n=15) mice. The data are expressed as the mean breaking point + S.E.M. for nicotine IVSA (30.0 μg/kg/infusion, *p<0.05). D) Dose-response curve for nicotine reinforcement in WT (n=11) and β4KO (n=9) mice. Mice were trained to respond for ascending doses of nicotine (7.5, 15, 30 and 60 μg/ kg/ infusion) and saline on an FR3 schedule of reinforcement. Results are expressed as mean number of nicotine infusions earned in 1 h ± S.E.M. for each dose during 3 days of training. Two-way repeated measures ANOVA followed by LSD post-hoc (*p<0.05, **p<0.01).

Figure 2. Basal and nicotine-stimulated extracellular DA levels in the NAC of β4KO and WT mice. A) Left hand side – Mean basal DA levels in WT (n=21) and β4KO (n=21) mice, + S.E.M. # p<0.05. Right hand side – Mean NAC DA levels following an injection of saline (s.c.) in WT (n=10) and β4KO (n=9) mice ± S.E.M. B – D) Change in NAC DA levels relative to baseline following an acute injection of nicotine (s.c.), at 0.17 mg/kg (B; WT n=10, KO n=9), 0.24 mg/kg (C; WT n=5, KO n=5) or 0.33 mg/kg (D; WT n=6, KO=7), at 15 min intervals up to 120 min post-injection. Data represented as mean ± S.E.M. Two-way repeated measures ANOVA followed by LSD post-hoc test. *p<0.05 vs. baseline; #p<0.05 genotype difference.

Figure 3. Nicotine-elicited VTA DAergic neuron responses *in vivo* in WT and β4KO mice. A) DAergic neurons' spontaneous firing frequency (left panel), and spontaneous bursting activity (right panel) in WT

(n=90) and β4KO mice VTA DA neurons (n=101). Mean + S.E.M. B) Top – a representative trace at 10 μg/kg/injection nicotine in a VTA DA neuron of a WT and β4KO mouse. Bottom - Increased variation from baseline in firing frequency for WT and β4KO mice injected with nicotine (0, 5, 10, 15, 30, 60 μg/kg/injection). Paired t-test vs. saline *p<0.05, ***p<0.001. C) Changes in proportion of spikes within bursts (SWB) in WT and β4KO mice injected with nicotine (0, 5, 10, 15, 30, 60 μg/kg/injection). Wilcoxon paired test vs. saline *p<0.05. Data represented as Median ± interquartile intervals. Dots represent outliers. The number of cells recorded is indicated on the graph.

Figure 4. Endogenous and exogenous expression of β4 in the mouse brain. A) PGK-β4 lentiviral vector for expression of β4 nAChR subunits and enhanced green fluorescent protein (eGFP). Sub-cloning by XhoI/BsrGI restriction enzyme digestion. ΔU3 - deletion in U3 of 3'LTR; LTR – long terminal repeat; PGK – phosphoglycerate kinase promotor; β4 – β4 WT mouse cDNA sequence; IRES – internal ribosome entry sequence; WPRE – woodchuck hepatitis B virus posttranscriptional response element. B) Autoradiography of heteromeric nAChRs (total I^{125}-epibatidine) and β4* nAChRs (I^{125}-epibatidine + 5-I-A85380) of MHb-injected (left) and IPN-injected (right) mice. WT-GFP and KO-GFP were injected with control GFP-only expressing lentivirus. C) Immunofluorescence staining of the IPN. Transgenic β4-cre mouse injected with an AAV for cre-dependent fluorophore expression (green). GFP (green) - green fluorescent protein; TH (blue) - tyrosine hydroxylase; ChAT (red) - choline acetyl transferase. D) Neuro-anatomical localization of lentiviral infection, and corresponding Franklin brain atlas images, visualized by the eGFP reporter protein in the MHb and IPN.

Figure 5. Effects of β4* nAChR re-expression in the MHb (A-B) and IPN (C-F) on nicotine IVSA and VTA DAergic neuron responses to nicotine. A) Mean ± S.E.M. number of intravenous nicotine infusions during 3 days for each dose of nicotine tested (7.5, 15.0, 30.0 and 60.0 μg/kg/infusion) on an FR3 reinforcement schedule in WT-GFP^{MHb} (n=9), KO-GFP^{MHb} (n=8) and KO-$\beta4^{MHb}$ (n=7) mice. Two-way repeated measures ANOVA with Tukey's post-hoc test (**p<0.01, group effect). The inset represents the quantification of 5-I-A85380-resistant I^{125}-epibatidine autoradiographic intensity in the MHb of KO-$\beta4^{MHb}$

mice. Data are the normalized mean inverse luminosity + S.E.M. relative to WT-GFP^{MHb} (n=6). KO-GFP^{MHb} (n=6), KO-β4^{MHb} (n=14). B) The mean + S.E.M. amount of nicotine consumed during the IVSA experiment (μg/kg), at each dose tested. One-way ANOVA with Tukey's post-hoc test. *p<0.05, **p<0.01, ns p>0.05. C) Mean ± S.E.M. number of intravenous nicotine infusions during 3 days for each dose of nicotine tested (7.50, 15.0, 30.0 and 60.0 μg/kg/infusion) on an FR3 reinforcement schedule in WT-GFP^{IPN} (n=5), KO-GFP^{IPN} (n=9) and KO-β4^{IPN} (n=9) mice. Two-way repeated measures ANOVA with Tukey's post-hoc test. ***p< 0.001 KO-GFP^{IPN} vs. WT-GFP^{IPN}, $$ p<0.01, $$$ p<0.001 KO-β4^{IPN} vs. KO-GFP^{IPN}, # p<0.05 KO-β4^{IPN} vs. WT-GFP^{IPN}. The inset represents the quantification of 5-I-A85380-resistant I^{125}-epibatidine autoradiographic intensity in the IPN. Data show the normalized mean inverse luminosity + S.E.M. relative to WT-GFP^{IPN} (n=4). KO-GFP^{IPN} (n=4), KO-β4^{IPN} (n=7). D) The mean amount of nicotine consumed during the IVSA experiment (μg/kg), at each dose tested. One-way ANOVA with Tukey's post-hoc test * p<0.05, ** p<0.01, ***p<0.001, ns p>0.05. E) Variation from baseline in firing frequency for WT-GFP^{IPN}, KO-GFP^{IPN} and KO-β4^{IPN} mice in response to nicotine (0, 10, 30 μg/kg/injection). Mean + S.E.M., t-test vs. saline *p<0.05, **p<0.01, ***p<0.001. F) Changes in the proportion of spikes within bursts (SWB) in WT-GFP^{IPN}, KO-GFP^{IPN} and KO-β4^{IPN} mice in response to nicotine (0, 10, 30 μg/kg/injection). Median ± interquartile intervals. Dots represent outliers. Wilcoxon paired test vs. saline. *p<0.05, **p<0.01. The number of cells recorded is annotated.

Supplementary Figure 1. Schematic representation of the experimental procedures stating ages, numbers and sources of mice, as well as the order, duration and location of experiments.

Supplementary Figure 2. Operant responding for food pellets and nicotine in WT and β4KO mice. A) Active and inactive nose-pokes for food pellets on an FR1 schedule of reinforcement during 8 days followed by an FR3 during 6 days in WT (n=41) and β4 KO (n=36) mice, and 3 days of re-training after catheter surgery (WT n=38, β4KO n=27). Results are expressed as mean number of nose-pokes in 1 h ± S.E.M. B) Nose-poking at the active and inactive hole during **nicotine** IVSA (30 μg/kg/infusion) over 10 days in WT (n=22) and β4KO (n=15) mice. Data represent mean ± S.E.M (*p<0.05; active hole

responding in WT vs β4KO mice). C-D) Nose-poking at the active and inactive hole during **nicotine** IVSA (30 μg/kg/infusion) over 6 days in MHb-injected (C; WT-GFP^{MHb} n=9, KO-GFP^{MHb} n=8, and KO-β4^{MHb} n=7) mice and IPN-injected (D; WT-GFP^{IPN} n=6, KO-GFP^{IPN} n=9, and KO-β4^{IPN} n=9) mice prior to nicotine IVSA dose-response analysis (Figure 5). Results are expressed as mean number of nicotine infusions in 1 h ± S.E.M. Three-way repeated measures ANOVA **p<0.01 and ***p<0.001 genotype effect. E) Nicotine IVSA in WT-GFP^{MHb}, KO-GFP^{MHb} and KO-β4^{MHb} re-expressing sub-threshold levels of β4 nAChRs in the MHb (*low expressers*, low expr.). Mean number of Infusions ± S.E.M. over the last 3 sessions at each dose of nicotine (0, 7.5, 15.0, 30.0, 60.0 μg/kg/infusion) tested on an FR3 schedule of reinforcement. WT-GFP^{MHb} (n=9), KO-GFP^{MHb} (n=8), KO-β4^{MHb} low expr (n=8) (WT-GFP^{MHb} vs KO-GFP^{MHb}, *p<0.05, **p<0.01, ***p<0.001, WT-GFP^{MHb} vs KO-β4^{MHb} low expr #p<0.05, ###p<0.001). The inset represents the quantification of 5-I-A85380-resistant I^{125}-epibatidine autoradiographic intensity in the IPN of mice trained on nicotine IVSA. Data are the normalized mean inverse luminosity + S.E.M. in KO-GFP^{MHb} (n=8) and KO-β4^{MHb} low expr (n=16) relative to to WT-GFP^{MHb} (n=6) mice (t-test, **p<0.01).

Supplementary Figure 3. Lentiviral vector-induced transgene expression in targeted structures and their terminals, and characterization of β4-expressing IPN neurons. A) PGK-GFP lentivirus targeted infection to the MHb (top). GFP expression (green, anti-GFP) in the MHb and at MHb neuron terminals in the IPN (bottom). Red - anti-choline acetyltransferase (ChAT). B) PGK-β4 lentivirus targeted infection to the MHb and 5-I-A85380-resistant I^{125}-epibatidine binding (putatively β4* nAChRs) in the MHb (left) and its terminals in the IPN (right) of KO-β4^{MHb} mice. Autoradiographs in MHb- and IPN-containing brain sections in the WT-GFP^{MHb} are from the same mouse, as is the case for KO-GFP^{MHb} and KO-β4^{MHb} brain sections. C) PGK-GFP lentivirus targeted infection to the IPN (top). GFP expression (green, anti-GFP) in the IPN and at IPN neuron terminals in the caudal dorsal raphe nucleus (cDRN) and the laterodorsal tegmentum (LDTg, bottom). Red - anti-choline acetyltransferase (ChAT). D) PGK-β4 lentivirus targeted infection to the IPN and 5-I-A85380-resistant I^{125}-epibatidine binding (putatively β4* nAChRs) in

the IPN (left) and modestly at the terminals in the LDTg (right) of a KO-β4^{IPN} mouse. Autoradiographs in IPN- and LDTg-containing brain sections in the WT-GFP^{IPN} are from the same mouse, as is the case for KO-GFP^{IPN} and KO-β4^{IPN} brain sections. E)-F) Visualization and characterization of β4cre-expressing neurons in the IPN. Transgenic β4cre mice injected with an AAV for cre-dependent fluorophore expression (green) in neurons expressing cre-recombinase, driven by β4 promoter. E) Proportion of β4cre-expressing neurons (GFP-positive) that colocalize with somatostatin immunolabelling. 360 GFP-positive cells were assessed across 16 brain sections at anterior/posterior (AP) position -3.6 and -3.8mm from bregma. n=5 mice. F) Immunofluorescence in the IPN revealing localization of β4-expressing neurons. α-GFP - anti-green fluorescent protein immunolabelling, revealing GCaMP5 expression (green); α-Sst - anti-somatostatin immunolabelling (red). G) Colocalization of GFP and somatostating staining demonstrates that the PGK-β4 lentivirus infects somatostatin neurons of the IPN.

REFERENCES

Antolin-Fontes B, Ables JL, Görlich A, Ibañez-Tallon I (2014). The habenulo-interpeduncular pathway in nicotine aversion and withdrawal. *Neuropharmacology*.

Beiranvand F, Zlabinger C, Orr-Urtreger a, Ristl R, Huck S, Scholze P (2014). Nicotinic acetylcholine receptors control acetylcholine and noradrenaline release in the rodent habenulo-interpeduncular complex. *British journal of pharmacology*: 1-41.

Bierut LJ, Stitzel Ja, Wang JC, Hinrichs AL, Grucza Ra, Xuei X, *et al* (2008). Variants in nicotinic receptors and risk for nicotine dependence. *The American journal of psychiatry* **165**: 1163-1171.

Dao DQ, Perez EE, Teng Y, Dani Ja, De Biasi M (2014). Nicotine Enhances Excitability of Medial Habenular Neurons via Facilitation of Neurokinin Signaling. *The Journal of neuroscience : the official journal of the Society for Neuroscience* **34**: 4273-4284.

Di Chiara G, Bassareo V, Fenu S, De Luca MA, Spina L, Cadoni C, *et al* (2004). Dopamine and drug addiction: the nucleus accumbens shell connection. *Neuropharmacology* **47 Suppl 1**: 227-241.

Fenster CP, Rains MF, Noerager B, Quick MW, Lester Ra (1997). Influence of subunit composition on desensitization of neuronal acetylcholine receptors at low concentrations of nicotine. *The Journal of neuroscience : the official journal of the Society for Neuroscience* **17**: 5747-5759.

Fields HL, Hjelmstad GO, Margolis EB, Nicola SM (2007). Ventral tegmental area neurons in learned appetitive behavior and positive reinforcement. *Annual review of neuroscience* **30**: 289-316.

Fowler CD, Kenny PJ (2013). Nicotine aversion: Neurobiological mechanisms and relevance to tobacco dependence vulnerability. *Neuropharmacology*: 1-12.

Frahm S, Slimak Ma, Ferrarese L, Santos-Torres J, Antolin-Fontes B, Auer S, *et al* (2011). Aversion to nicotine is regulated by the balanced activity of β4 and α5 nicotinic receptor subunits in the medial habenula. *Neuron* **70**: 522-535.

Gallego X, Cox RJ, Laughlin JR, Stitzel Ja, Ehringer Ma (2013). Alternative CHRNB4 3'-UTRs mediate the allelic effects of SNP rs1948 on gene expression. *PloS one* **8**: e63699.

Geisler S, Zahm DS (2005). Afferents of the ventral tegmental area in the rat-anatomical substratum for integrative functions. *The Journal of comparative neurology* **490**: 270-294.

Glick SD, Sell EM, McCallum SE, Maisonneuve IM (2011). Brain regions mediating α3β4 nicotinic antagonist effects of 18-MC on nicotine self-administration. *European Journal of Pharmacology* **669**: 71-75.

Görlich A, Antolin-Fontes B, Ables JL, Frahm S, Slimak Ma, Dougherty JD, *et al* (2013). Reexposure to nicotine during withdrawal increases the pacemaking activity of cholinergic habenular neurons. *Proceedings of the National Academy of Sciences of the United States of America* **110**: 17077-17082.

Grady SR, Moretti M, Zoli M, Marks MJ, Zanardi A, Pucci L, *et al* (2009). Rodent habenulo-interpeduncular pathway expresses a large variety of uncommon nAChR subtypes, but only the alpha3beta4* and alpha3beta3beta4* subtypes mediate acetylcholine release. *The Journal of neuroscience : the official journal of the Society for Neuroscience* **29**: 2272-2282.

Groenewegen HJ, Ahlenius S, Haber SN, Kowall NW, Nauta WJ (1986). Cytoarchitecture, fiber connections, and some histochemical aspects of the interpeduncular nucleus in the rat. *The Journal of comparative neurology* **249**: 65-102.

Haller G, Druley T, Vallania FL, Mitra RD, Li P, Akk G, *et al* (2012). Rare missense variants in CHRNB4 are associated with reduced risk of nicotine dependence. *Human Molecular Genetics* **21**: 647-655.

Hansen SB, Sulzenbacher G, Huxford T, Marchot P, Taylor P, Bourne Y (2005). Structures of Aplysia AChBP complexes with nicotinic agonists and antagonists reveal distinctive binding interfaces and conformations. *The EMBO journal* **24**: 3635-3646.

Hartmann-Boyce J, Stead LF, Cahill K, Lancaster T (2013). Efficacy of interventions to combat tobacco addiction: Cochrane update of 2012 reviews. *Addiction* **108**: 1711-1721.

Hsu Y-Wa, Tempest L, Quina La, Wei aD, Zeng H, Turner EE (2013). Medial Habenula Output Circuit Mediated by 5 Nicotinic Receptor-Expressing GABAergic Neurons in the Interpeduncular Nucleus. *Journal of Neuroscience* **33**: 18022-18035.

Hsu Y-Wa, Wang SD, Wang S, Morton G, Zariwala Ha, de la Iglesia HO*, et al* (2014). Role of the dorsal medial habenula in the regulation of voluntary activity, motor function, hedonic state, and primary reinforcement. *The Journal of neuroscience : the official journal of the Society for Neuroscience* **34**: 11366-11384.

Jackson KJ, Sanjakdar SS, Muldoon PP, McIntosh JM, Damaj MI (2013). The α3β4* nicotinic acetylcholine receptor subtype mediates nicotine reward and physical nicotine withdrawal signs independently of the α5 subunit in the mouse. *Neuropharmacology* **70**: 228-235.

Kobayashi Y, Sano Y, Vannoni E, Goto H, Suzuki H, Oba A*, et al* (2013). Genetic dissection of medial habenula-interpeduncular nucleus pathway function in mice. *Frontiers in behavioral neuroscience* **7**: 17.

Maskos U, Molles BE, Pons S, Besson M, Guiard BP, Guilloux J-P*, et al* (2005). Nicotine reinforcement and cognition restored by targeted expression of nicotinic receptors. *Nature* **436**: 103-107.

Messer K, Trinidad DR, Al-Delaimy WK, Pierce JP (2008). Smoking cessation rates in the United States: A comparison of young adult and older smokers. *American Journal of Public Health* **98**: 317-322.

Morel C, Fattore L, Pons S, Hay Ya, Marti F, Lambolez B*, et al* (2014). Nicotine consumption is regulated by a human polymorphism in dopamine neurons. *Molecular psychiatry*: 1-7.

Orejarena MJ, Herrera-Solís A, Pons S, Maskos U, Maldonado R, Robledo P (2012). Selective re-expression of β2 nicotinic acetylcholine receptor subunits in the ventral tegmental area of the mouse restores intravenous nicotine self-administration. *Neuropharmacology* **63**: 235-241.

Paxinos G, Franklin K (2004). *The mouse brain in stereotaxic coordinates* Elseiver Academic: San Diego.

Ren J, Qin C, Hu F, Tan J, Qiu L, Zhao S*, et al* (2011). Habenula "cholinergic" neurons co-release glutamate and acetylcholine and activate postsynaptic neurons via distinct transmission modes. *Neuron* **69**: 445-452.

Saccone NL, Wang JC, Breslau N, Johnson EO, Hatsukami D, Saccone SF*, et al* (2009). The CHRNA5-CHRNA3-CHRNB4 nicotinic receptor subunit gene cluster affects risk for nicotine dependence in African-Americans and in European-Americans. *Cancer research* **69**: 6848-6856.

Salas R, Pieri F, De Biasi M (2004). Decreased signs of nicotine withdrawal in mice null for the beta4 nicotinic acetylcholine receptor subunit. *The Journal of neuroscience : the official journal of the Society for Neuroscience* **24**: 10035-10039.

Salas R, Pieri F, Fung B, Dani Ja, De Biasi M (2003). Altered anxiety-related responses in mutant mice lacking the beta4 subunit of the nicotinic receptor. *The Journal of neuroscience : the official journal of the Society for Neuroscience* **23**: 6255-6263.

Salas R, Sturm R, Boulter J, De Biasi M (2009). Nicotinic receptors in the habenulo-interpeduncular system are necessary for nicotine withdrawal in mice. *The Journal of neuroscience : the official journal of the Society for Neuroscience* **29**: 3014-3018.

Sanchis-Segura C, Spanagel R (2006). Behavioural assessment of drug reinforcement and addictive features in rodents: an overview. *Addict Biol* **11**(1): 2-38.

Schlaepfer IR, Hoft NR, Collins AC, Corley RP, Hewitt JK, Hopfer CJ*, et al* (2008). The CHRNA5/A3/B4 gene cluster variability as an important determinant of early alcohol and tobacco initiation in young adults. *Biological psychiatry* **63**: 1039-1046.

Slimak Ma, Ables JL, Frahm S, Antolin-Fontes B, Santos-Torres J, Moretti M*, et al* (2014). Habenular expression of rare missense variants of the β4 nicotinic receptor subunit alters nicotine consumption. *Frontiers in human neuroscience* **8**: 12.

Suto N, Wise RA (2011). Satiating effects of cocaine are controlled by dopamine actions in the nucleus accumbens core. *J Neurosci* **31**(49): 17917-17922.

Tolu S, Eddine R, Marti F, David V, Graupner M, Pons S*, et al* (2013). Co-activation of VTA DA and GABA neurons mediates nicotine reinforcement. *Molecular psychiatry* **18(3)**: 382-393.

Ungless MA, Grace AA (2012). Are you or aren't you? Challenges associated with physiologically identifying dopamine neurons. *Trends Neurosci* **35**(7): 422-430.

Walters CL, Brown S, Changeux JP, Martin B, Damaj MI (2006). The β2 but not α7 subunit of the nicotinic acetylcholine receptor is required for nicotine-conditioned place preference in mice. *Psychopharmacology* **184**: 339-344.

World Health Organization W (2013). WHO report on the global tobacco epidemic. Vol 2015.

Xu W, Orr-Urtreger a, Nigro F, Gelber S, Sutcliffe CB, Armstrong D*, et al* (1999). Multiorgan autonomic dysfunction in mice lacking the beta2 and the beta4 subunits of neuronal nicotinic acetylcholine receptors. *The Journal of neuroscience : the official journal of the Society for Neuroscience* **19**: 9298-9305.

Yamaguchi T, Danjo T, Pastan I, Hikida T, Nakanishi S (2013). Distinct roles of segregated transmission of the septo-habenular pathway in anxiety and fear. *Neuron* **78**: 537-544.

Zhao-Shea R, Liu L, Pang X, Gardner PD, Tapper AR (2013). Activation of GABAergic neurons in the interpeduncular nucleus triggers physical nicotine withdrawal symptoms. *Current biology : CB* **23**: 2327-2335.

Figure 1

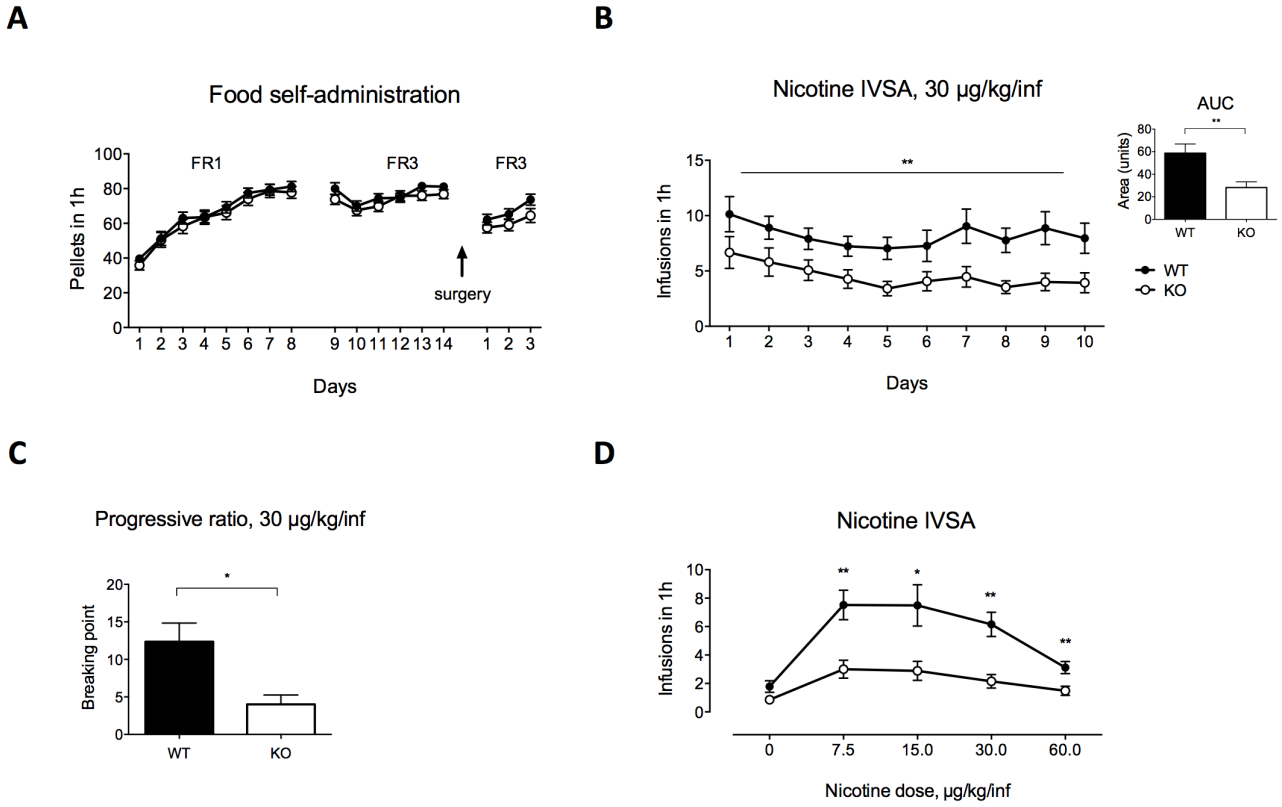
A
Food self-administration
Pellets in 1h
FR1
FR3
FR3
surgery
Days
B
Nicotine IVSA, 30 µg/kg/inf
Infusions in 1h
Days
AUC
Area (units)
WT
KO
C
Progressive ratio, 30 µg/kg/inf
Breaking point
WT
KO
D
Nicotine IVSA
Infusions in 1h
Nicotine dose, µg/kg/inf

Figure 2

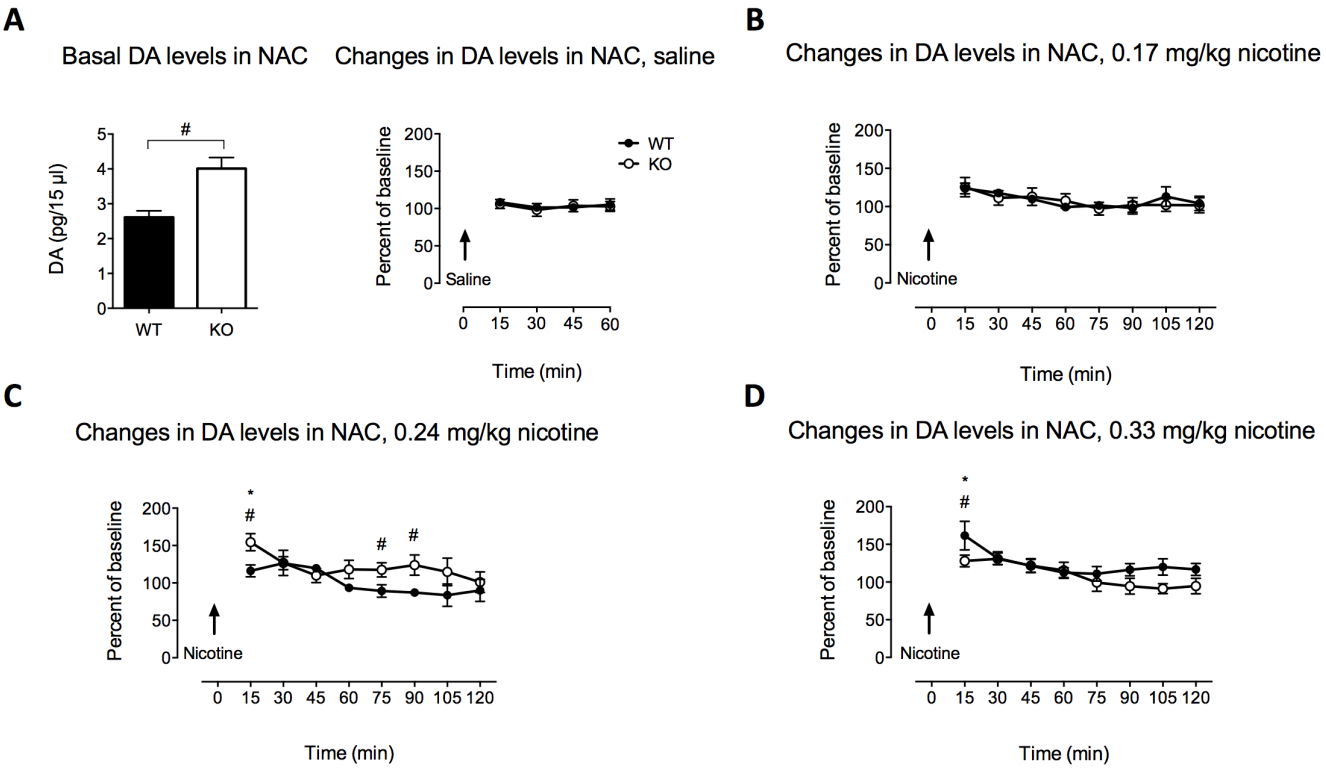
A
Basal DA levels in NAC
Changes in DA levels in NAC, saline
DA (pg/15 µl)
WT
KO
Percent of baseline
Saline
Time (min)
B
Changes in DA levels in NAC, 0.17 mg/kg nicotine
Nicotine
C
Changes in DA levels in NAC, 0.24 mg/kg nicotine
D
Changes in DA levels in NAC, 0.33 mg/kg nicotine

Figure 3

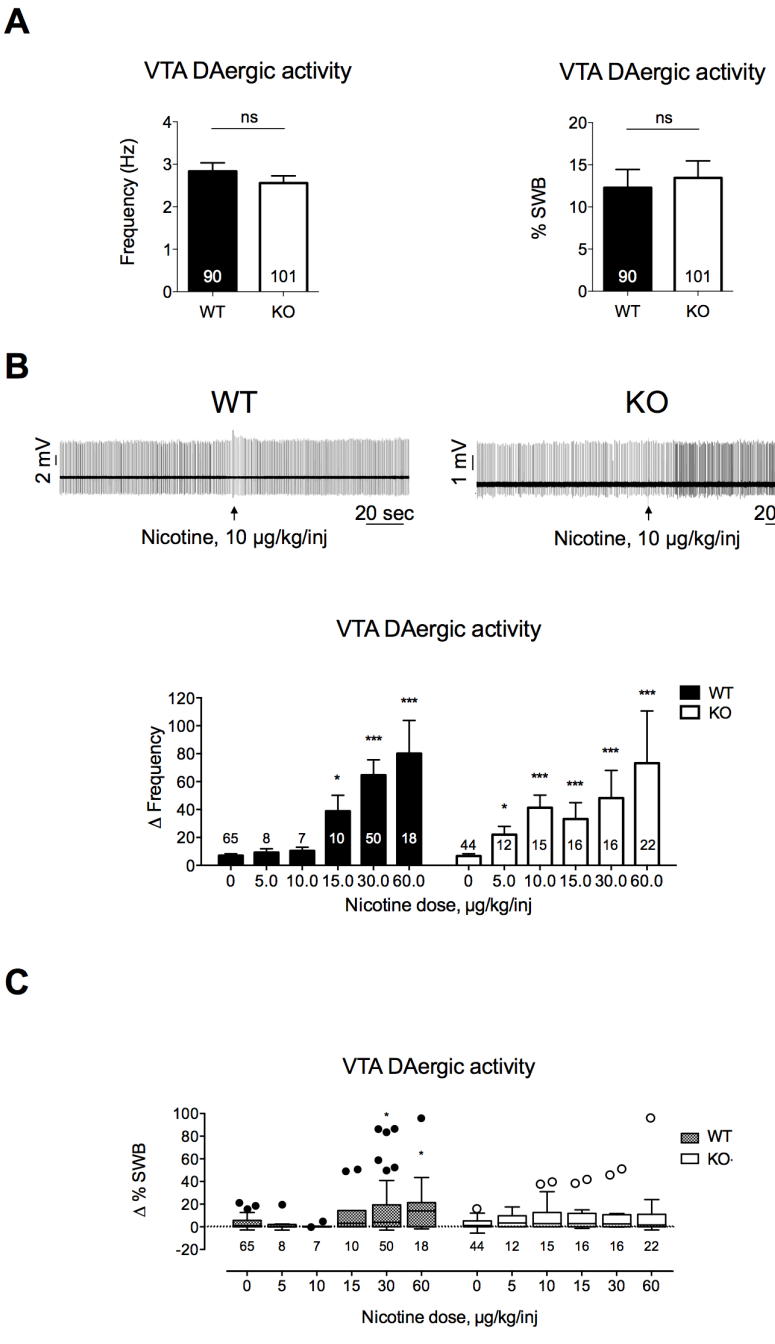
A
VTA DAergic activity
Frequency (Hz)
ns
90
101
WT
KO
VTA DAergic activity
% SWB
ns
90
101
WT
KO
B
WT
KO
2 mV
1 mV
20 sec
Nicotine, 10 µg/kg/inj
20 sec
Nicotine, 10 µg/kg/inj
VTA DAergic activity
Δ Frequency
WT
KO
65 8 7 10 50 18
44 12 15 16 16 22
0 5.0 10.0 15.0 30.0 60.0
0 5.0 10.0 15.0 30.0 60.0
Nicotine dose, µg/kg/inj
C
VTA DAergic activity
Δ % SWB
WT
KO
65 8 7 10 50 18
44 12 15 16 16 22
0 5 10 15 30 60
0 5 10 15 30 60
Nicotine dose, µg/kg/inj

Figure 4

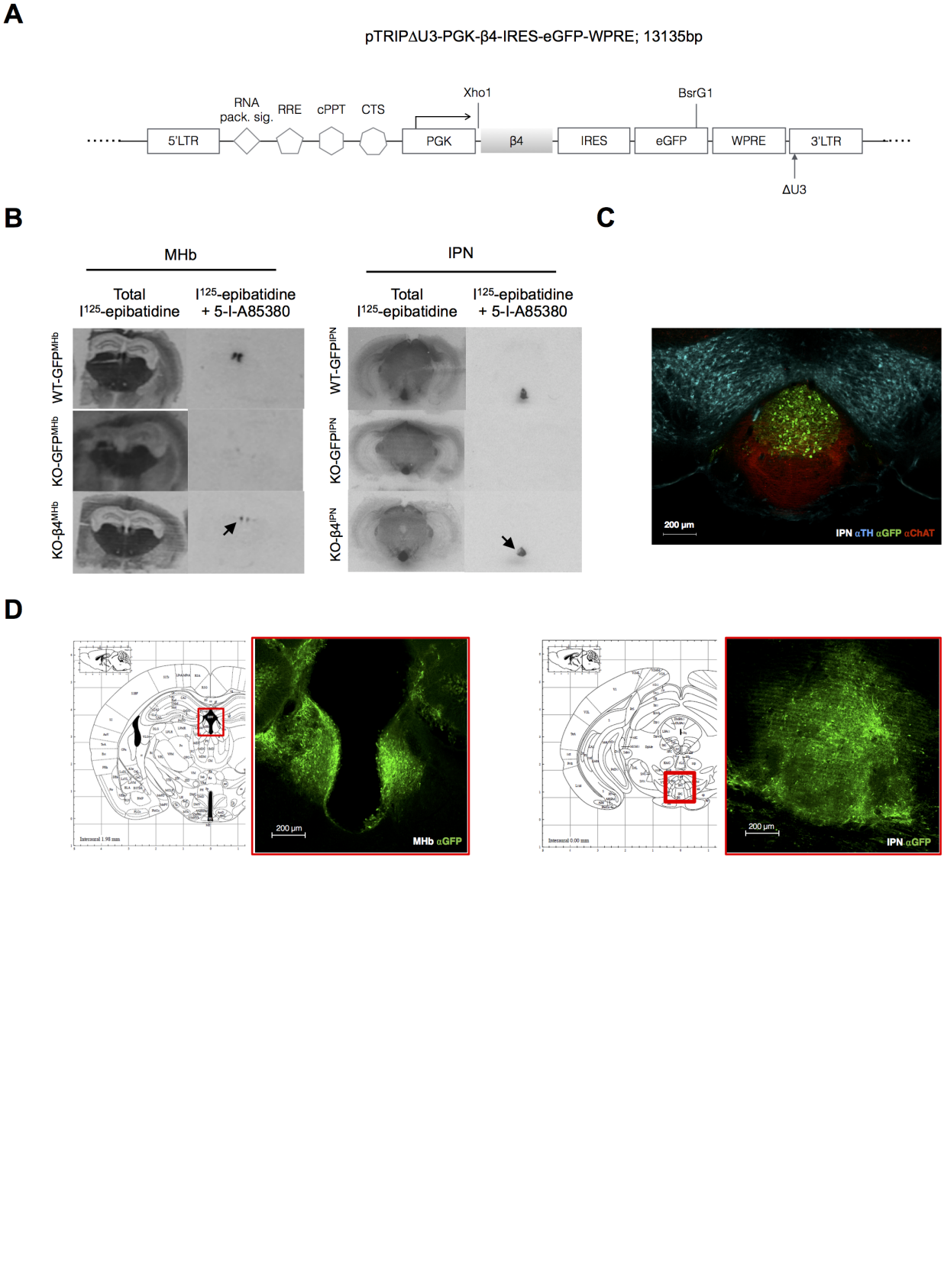
A
pTRIPΔU3-PGK-β4-IRES-eGFP-WPRE; 13135bp
RNA pack. sig.
RRE
cPPT
CTS
Xho1
BsrG1
5'LTR
PGK
β4
IRES
eGFP
WPRE
3'LTR
ΔU3
B
MHb
IPN
Total I125-epibatidine
I125-epibatidine + 5-I-A85380
WT-GFPMHb
KO-GFPMHb
KO-β4MHb
WT-GFPIPN
KO-GFPIPN
KO-β4IPN
C
200 µm
IPN αTH αGFP αChAT
D
200 µm
MHb αGFP
200 µm
IPN αGFP

Figure 5

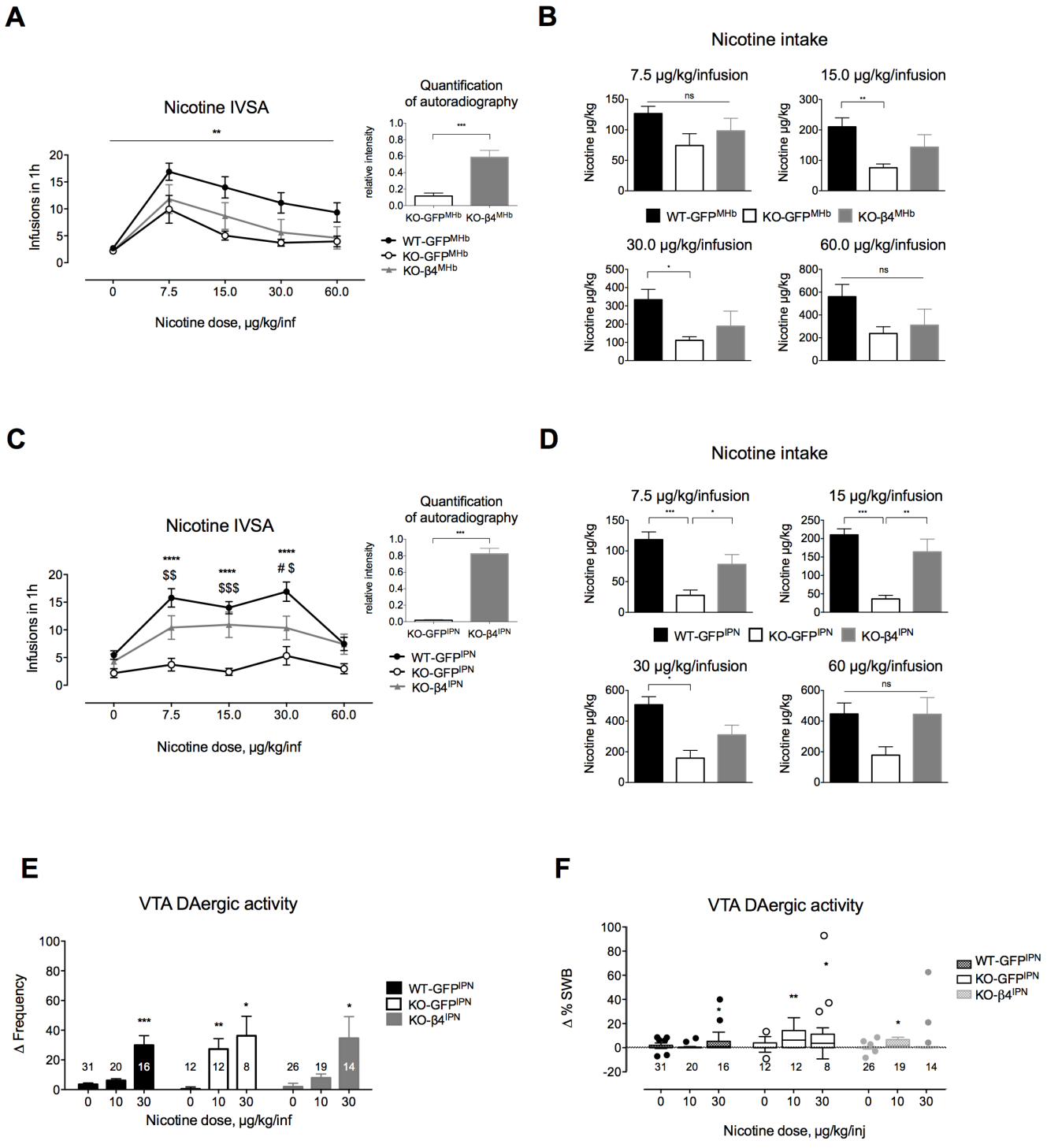
A
Nicotine IVSA
Infusions in 1h
Nicotine dose, µg/kg/inf
Quantification of autoradiography
relative intensity
KO-GFPMHb
KO-β4MHb
WT-GFPMHb
KO-GFPMHb
KO-β4MHb
B
Nicotine intake
7.5 µg/kg/infusion
15.0 µg/kg/infusion
30.0 µg/kg/infusion
60.0 µg/kg/infusion
Nicotine µg/kg
ns
WT-GFPMHb
KO-GFPMHb
KO-β4MHb
C
Nicotine IVSA
Infusions in 1h
Nicotine dose, µg/kg/inf
Quantification of autoradiography
relative intensity
KO-GFPIPN
KO-β4IPN
WT-GFPIPN
KO-GFPIPN
KO-β4IPN
D
Nicotine intake
7.5 µg/kg/infusion
15 µg/kg/infusion
30 µg/kg/infusion
60 µg/kg/infusion
Nicotine µg/kg
ns
WT-GFPIPN
KO-GFPIPN
KO-β4IPN
E
VTA DAergic activity
Δ Frequency
Nicotine dose, µg/kg/inf
WT-GFPIPN
KO-GFPIPN
KO-β4IPN
F
VTA DAergic activity
Δ % SWB
Nicotine dose, µg/kg/inj
WT-GFPIPN
KO-GFPIPN
KO-β4IPN

Supplementary figure 1

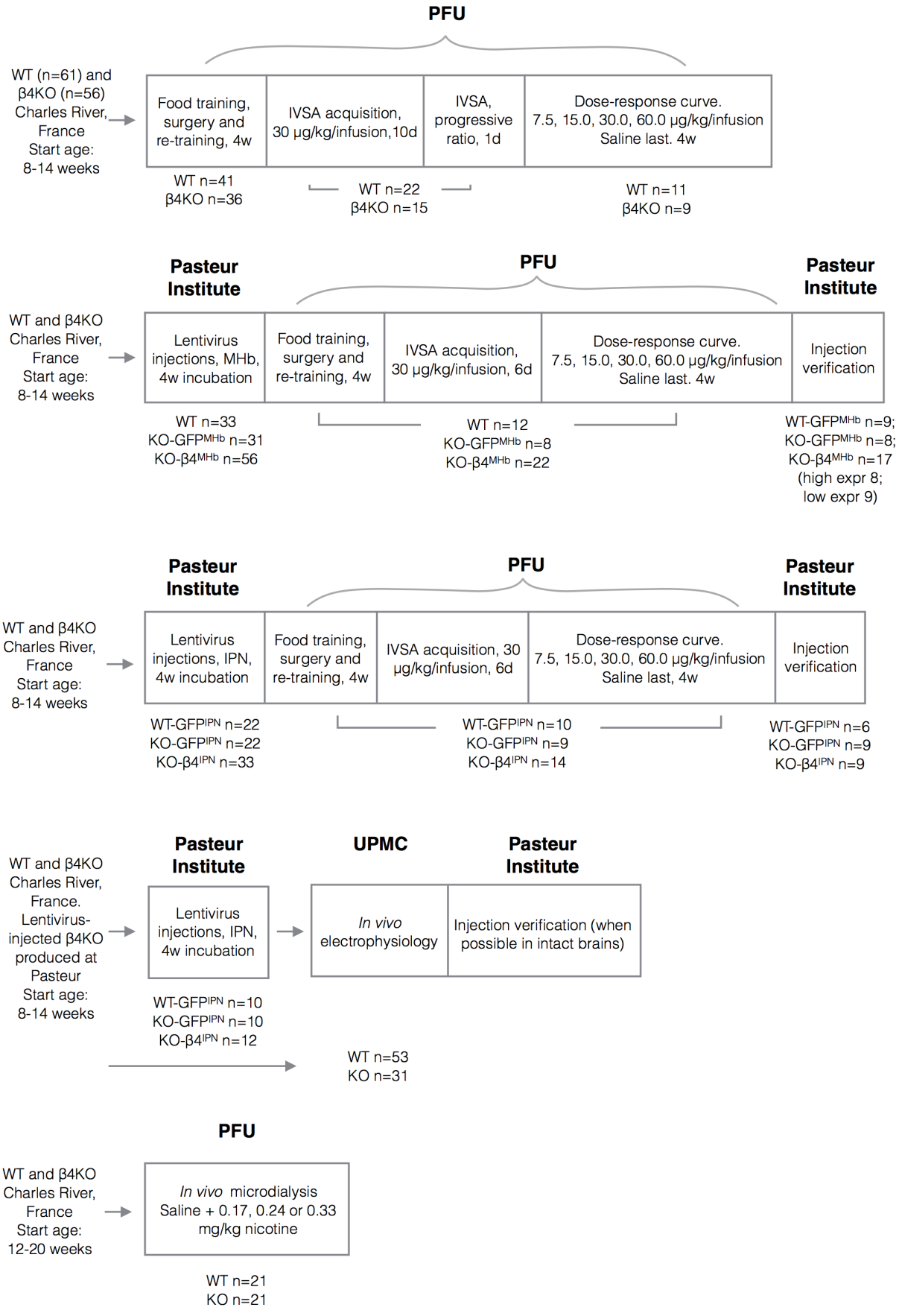

Supplementary figure 2

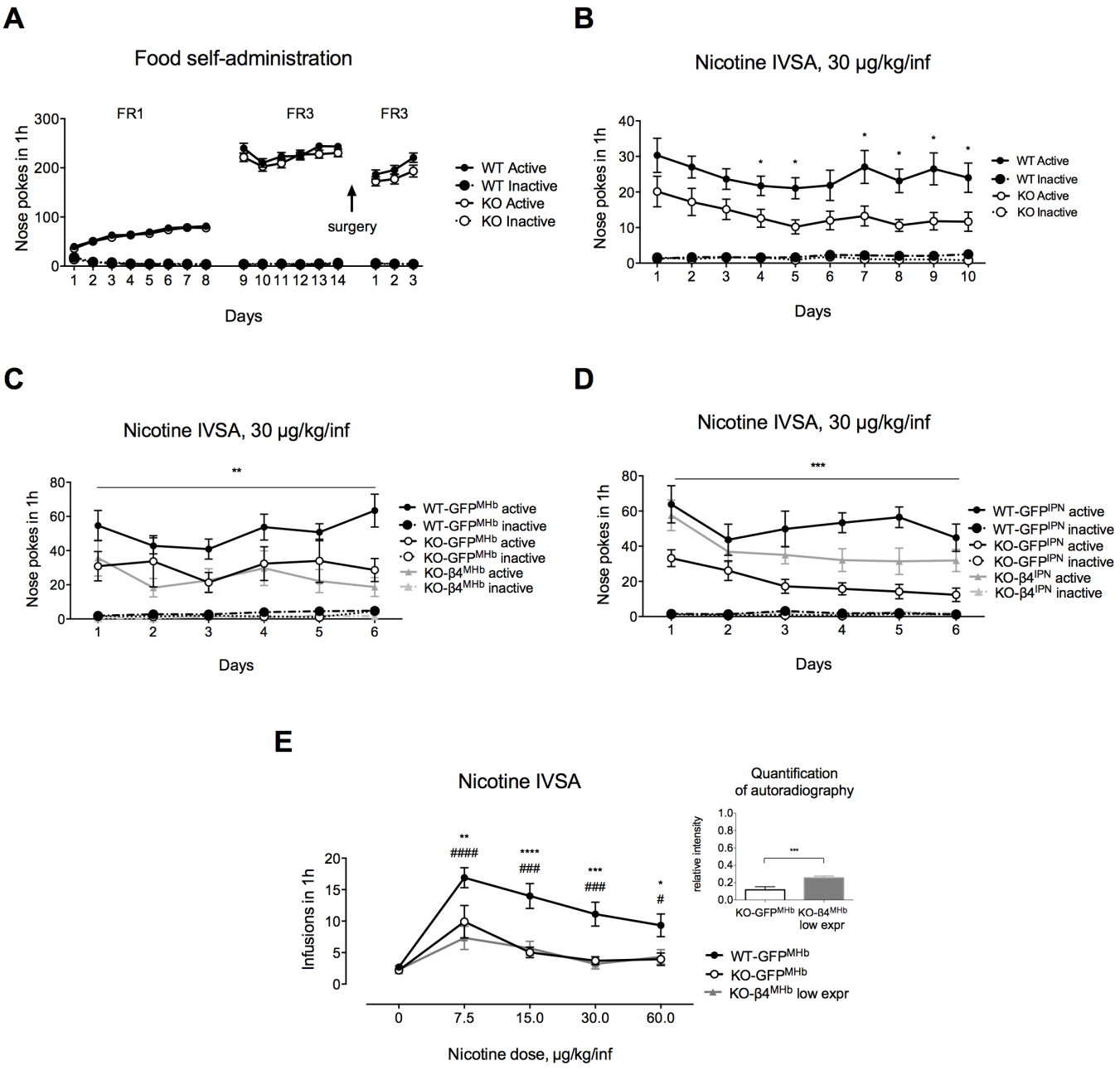

Supplementary figure 3